

Article

# Experimental and Numerical Study of Nonlinear Lamb Waves of a Low-Frequency $S_0$ Mode in Plates with Quadratic Nonlinearity

Xiangyan Ding <sup>1</sup>, Youxuan Zhao <sup>1,\*</sup> , Ning Hu <sup>1,2,\*</sup> , Yaolu Liu <sup>1</sup>, Jun Zhang <sup>1</sup> and Mingxi Deng <sup>1</sup> 

<sup>1</sup> College of Aerospace Engineering, Chongqing University, Chongqing 400044, China; dingxiangyan@cqu.edu.cn (X.D.); liuyaolu@cqu.edu.cn (Y.L.); mejzhang@cqu.edu.cn (J.Z.); dengmx65@yahoo.com (M.D.)

<sup>2</sup> State Key Laboratory of Coal Mine Disaster Dynamics and Control, Chongqing University, Chongqing 400044, China

\* Correspondence: youxuan.zhao@cqu.edu.cn (Y.Z.); ninghu@cqu.edu.cn (N.H.)

Received: 2 October 2018; Accepted: 23 October 2018; Published: 25 October 2018



**Abstract:** This paper investigates the propagation of low-frequency  $S_0$  mode Lamb waves in plates with quadratic nonlinearity through numerical simulations and experimental measurements. Both numerical and experimental results manifest distinct ultrasonic nonlinear behavior which is mainly presented by the second harmonics. Meanwhile, we find that both the acoustic nonlinearity parameter and dispersion distance show the exponential decay trend with the increase of frequency-thickness. Moreover, the results reveal that the frequency is key to affect the acoustic nonlinearity parameter and dispersion distance with the same frequency-thickness. This study theoretically and experimentally reveals that nonlinear Lamb waves of the low-frequency  $S_0$  mode are feasible to quantitatively identify material weak nonlinearity in plates.

**Keywords:** ultrasonic nonlinearity; lamb waves;  $S_0$  mode; numerical simulation; experiment

## 1. Introduction

The safety and durability of the key engineering structures, e.g., airplanes, pressure vessels, and high-speed trains, have been paid extensive attention to. Due to fatigue load, material degradation, the initiation and propagation of micro-cracks, micro-voids, etc. can often occur in those engineering structures in service life. Thus, there is an increasing demand to detect those small-scale defects using non-destructive testing methods.

Because of the low sensitivity, conventional linear ultrasonic technology could be difficult to detect the above defects [1–3]. However, nonlinear ultrasonic technologies [4–14] are dramatically sensitive to material microstructures, which could be promising in overcoming this problem. Especially nonlinear Lamb-wave detection techniques [15–39], which can be employed for long-range monitoring and inspection in thin plate structures, have attracted extensive attention in the past two decades.

Many efforts have been devoted to characterizing the micro-crack detection and early material degradation by higher harmonics of Lamb waves. Liu et al. [15] investigated experimentally the nonlinear acoustic effect on the crack depth. Shen et al. [16] numerically analyzed the process of Lamb waves interactions with fatigue cracks which can cause the nonlinear effect of higher harmonics and mode conversion. Deng et al. [17,18] and Matsuda et al. [19] declared that the matching phase velocities of fundamental and double frequency Lamb waves is necessary for an obvious second harmonic generation. Some researchers discussed the appropriate mode pairs for generation of the cumulative second harmonics in the circular tube damage/degradation quantitative assessment

application [20,21]. Li et al. [22] found that the second harmonic generation of the circumferential guided wave is more sensitive to changes in the interfacial properties. Bermes et al. [23,24] measured second harmonic effects of Lamb waves in a metallic plate through a time-frequency representation with a hybrid wedge generation and laser interferometric detection system. In most studies, the  $S_1$  and  $A_1$  [25,26] modes are commonly used as the fundamental waves because the phase velocities of these two modes can be easily matched. Definitely,  $S_0$  and  $A_0$  modes [27–30] have great advantages due to the higher energy and longer-distance propagation. Castaings et al. [29] studied the interaction of the low order  $A_0$  and  $S_0$  with vertical cracks in aluminum plates. Hu et al. [30] investigated the nonlinear effects of low-frequency  $S_0$  Lamb wave in thin plates with randomly distributed micro-cracks through numerical simulations. Meanwhile, the nonlinear mixing wave method for Lamb waves has also been developed to evaluate material nonlinearity and micro-cracks. Jiao et al. [31] reported the application of nonlinear Lamb wave-mixing method to detect the micro-cracks in plates. Ishii et al. [32] have theoretically investigated the non-collinear interaction of plate wave modes when the nonlinear wave is propagating in elastic plates. Zhao et al. [33] applied one-way collinear mixing method to numerically investigate the propagation of Lamb waves in thin plates with quadratic nonlinearity.

The low-frequency Lamb waves could introduce higher energy and a longer propagating distance. However, the experimental studies on the  $S_0$  and  $A_0$  modes Lamb waves are still rarely reported. It is also a challenge to select a feasible frequency for characterizing material weak nonlinearity accurately and effectively by a low-frequency  $S_0$  mode Lamb wave. Therefore, in this work, we aim to numerically and experimentally investigate the propagation of the  $S_0$  mode Lamb wave at lower-frequency (200 kHz) in plates with quadratic nonlinearity. The relationship between dispersion distance and frequency-thickness is explored, and the influence of the frequency on the dispersion distance with the same frequency-thickness is further discussed.

## 2. Nonlinear Lamb Waves

The dispersion is a representative characteristic of Lamb waves which means that the velocity of Lamb wave depends on material properties and the frequencies of the waves. Figure 1 shows the dispersion curves of Lamb wave in an aluminum plate with a 2 mm thickness.

Lamb waves usually process various wave modes. However, it is crucial to select an appropriate mode with the characteristics of a long propagating distance, low energy attenuation, and stabilized mode in engineering applications. It is well-known that the  $S_0$  and  $A_0$  modes Lamb wave can carry more energy with a smaller energy attenuation. Figure 1 indicates that only the  $S_0$  and  $A_0$  modes exist in the low-frequency domain (0–1600 kHz·mm). Meanwhile, some studies have demonstrated that the phase velocity matching is one necessary condition to accumulate the second harmonic. Additionally, the velocity mismatch between the fundamental wave and second harmonic can lead to an asynchronous interaction, which is the reason for the sinusoidal behavior named as dispersion distance  $L$  [40]:

$$L = \frac{2\pi}{|k_d|}, k_d = k(2\omega) - 2k(\omega) \quad (1)$$

where  $k$  is the wave number. When  $k_d$  is small enough, the phase velocities of the fundamental wave and second harmonic are approximately equal. The resonance condition can be achieved and  $L$  can increase linearly to the critical value. Additionally, the linear accumulative distance commonly used in practice is 25% of the dispersion distance [28]. It is clear that the phase velocity of the  $S_0$  mode basically slowly changes in the low-frequency domain (0–800 kHz·mm) in Figure 1a. Thus, it is appropriate to choose the  $S_0$  mode in the frequency domain (0–800 kHz·mm) to evaluate the early material degradation based on second harmonic generation. In engineering applications, it is essential to validate the relationship between frequency-thickness and dispersion distance. However, the research on that is still rarely reported. Here, we investigate the potential of the  $S_0$  mode from the frequency range of 0–800 kHz·mm through numerical simulations and experimental measurements.

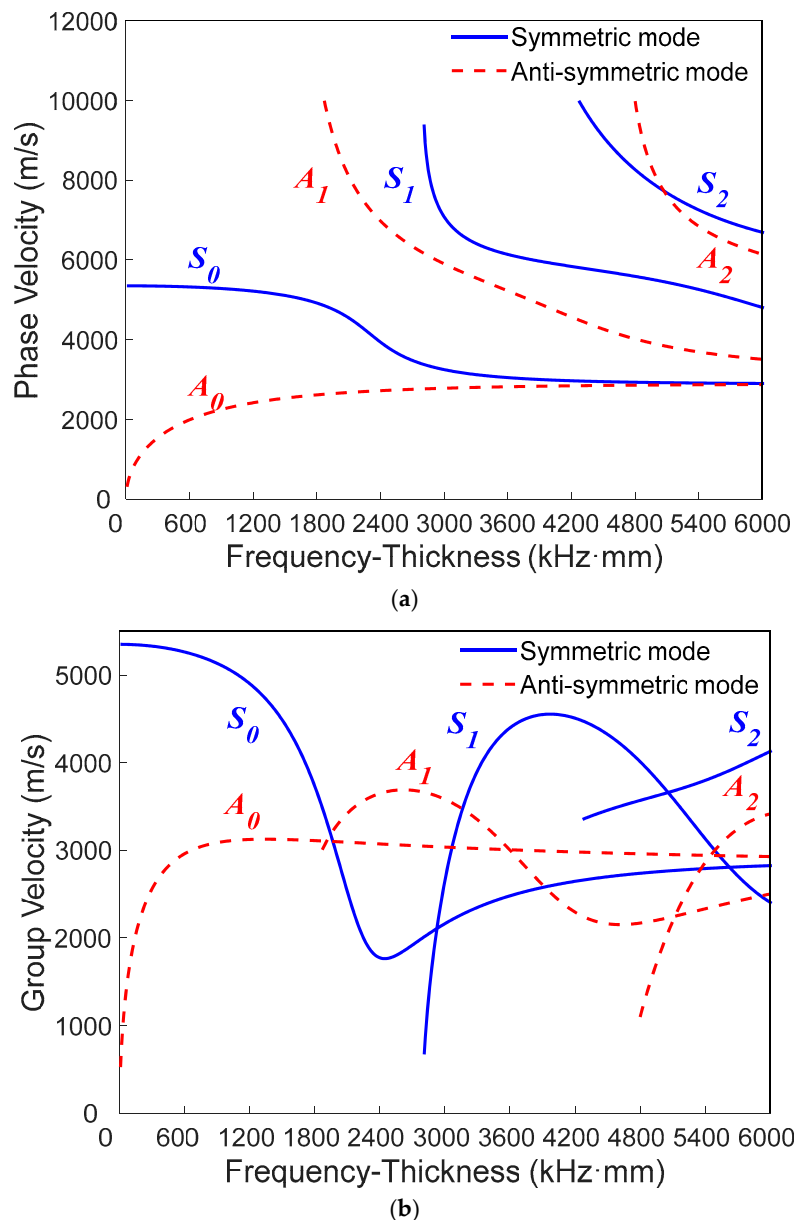


**Figure 1.** The dispersion curves of Lamb waves in an aluminum plate with a 2-mm thickness: (a) phase velocity; (b) group velocity.

### 3. Numerical Simulation

The two-dimensional finite element model (FEM) is constructed to simulate the Lamb wave propagation in a plate with a quadratic material nonlinearity by the commercial FEM software ABAQUS (Version 6.14, Dassault Systèmes Simulia Corp., Providence, RI, USA).

The problem of  $S_0$  mode Lamb waves propagating in a plate with a quadratic material nonlinearity is shown in Figure 2. An  $S_0$  mode wave pulse is generated by a dynamic displacement excitation on the left edge of the plate. The wave propagates along the  $x$  positive direction. Because of a quadratic nonlinearity, the second harmonic wave of the  $S_0$  mode is generated during the propagation of the fundamental  $S_0$  mode wave and finally received at different detection locations (the length  $D$  with a uniformly-spaced arrangement,  $D$  in this work is 25 mm).

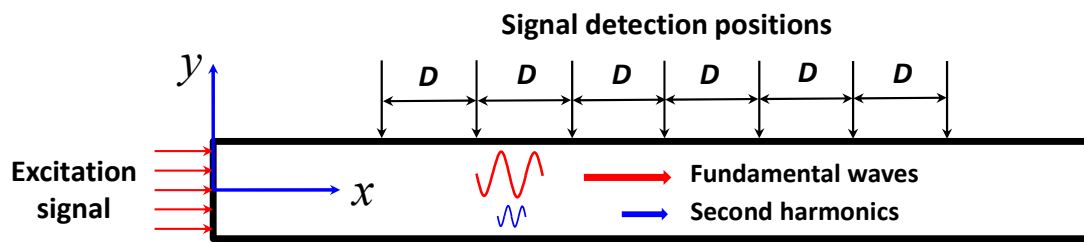


Figure 2. The schematic of Lamb waves propagation in a plate.

The quadratic nonlinear elastic constitutive law with third-order constants is used [39], which is expressed using Voigt’s notation  $C_{ijkl} = c_{IJ}$ ,  $C_{ijklmn} = c_{IJK}$ :

$$\sigma_{ij} = C_{ijkl}E_{kl} + \frac{1}{2}C_{ijklmn}E_{kl}E_{mn}, \tag{2}$$

$$C_{ijkl} = \lambda\delta_{ij}\delta_{kl} + \mu(\delta_{ik}\delta_{jl} + \delta_{il}\delta_{jk}), \tag{3}$$

$$C_{ijklmn} = (2l - 2m + n)\delta_{ij}\delta_{kl}\delta_{mn} + (2m - n)(\delta_{ij}I_{klmn} + \delta_{kl}I_{mnij} + \delta_{mn}I_{ijkl}) + \frac{n}{2}(\delta_{ik}I_{jlmn} + \delta_{il}I_{jkmn} + \delta_{jk}I_{ilmn} + \delta_{jl}I_{ikmn}). \tag{4}$$

where  $l$ ,  $m$ , and  $n$  are the Murnaghan third-order elastic constants and  $E$  is the Lagrangian or Green strain,  $I, J, K \in \{1, 2, 3, 4, 5, 6\}$ ,  $ij = 11, 22, 33, 23, 31, 12 \leftrightarrow I = 1, 2, 3, 4, 5, 6$ .

The material properties of the aluminum (AL-6061-T6) plate used in the simulations are listed in Table 1. Considering the computational accuracy, each highest frequency wavelength requires at least 20 elements. The element size in simulations is set to  $L_{max} = 0.2$  mm for the highest frequency 1200 kHz (the fundamental frequency is 600 kHz). The simulations with element size 0.15 mm and 0.1 mm are also investigated, which show the coincident accuracy but longer calculation time. Therefore, it is appropriate to select the element size as 0.2 mm for balancing the computational cost and accuracy. The rectangular region of 1000 mm  $\times$  2 mm is discretized by 50,000 four-node plane strain (CPE4R) elements in the FEM model.

Table 1. The mechanical parameters of aluminum AL-6061-T6.

$\rho$ (kg/m <sup>3</sup> )	$\lambda$ (MPa)	$\mu$ (MPa)	$l$ (MPa)	$m$ (MPa)	$n$ (MPa)
2704	$5.11 \times 10^4$	$2.63 \times 10^4$	$-2.82 \times 10^5$	$-3.39 \times 10^5$	$-4.16 \times 10^5$

ABAQUS/Explicit solver based on the central difference method is employed to solve the Lamb wave propagation in the time domain, which is conditionally stable. To ensure the accuracy of the solution, the stable time increment should be carefully chosen according to the time of the stress waves passing through the minimum element ( $3.9 \times 10^{-8}$  s). Therefore, considering the efficiency and the accuracy, the stable time increment is set to  $\Delta t = 1.0 \times 10^{-9}$ s. Meanwhile, a double precision operation is also performed to reduce the accumulative error.

The left edge of the plate is applied a dynamic displacement excitation which is a tone-burst signal and can be expressed as  $u(x, t) = A_0 \sin(2\pi ft) \times \sin(\pi ft/10)^2$ , where  $A_0$  is the amplitude of excitation signal ( $1 \times 10^{-4}$  mm in this study [33,41]), and  $f$  is the frequency of excitation signal. The fundamental wave and second harmonic are collected at the detection positions. In addition, the distance between from the left edge to the right edge is large enough to maximally eliminate the influence of boundary reflection.

Moreover, the acoustic nonlinearity parameter  $\beta = A_2/A_1^2$  [24] is used in this work, where  $A_1$  is the amplitude of the fundamental wave, and  $A_2$  is that of second harmonic.

Based on the concept mentioned in Section 2, we investigate the varying frequency-thickness cases with a constant 300 kHz and varying thickness (1.0–5.5 mm with the step of 0.5 mm). Additionally, cases of the same frequency-thickness (600 kHz·mm) with varying frequency are explored. More numerical case studies are not presented in this paper due to the same tendency.

#### 4. Experimental Measurement

In this section, a large number of experiments are employed to investigate the nonlinear behavior of Lamb waves. The schematic of the experimental setup is shown in Figure 3. A modular ultrasonic system RAM-5000 SNAP (RITEC Inc., Warwick, RI, USA) high power gated amplifier with two “RF burst” channels is used for the generation and detection of the nonlinear Lamb waves.

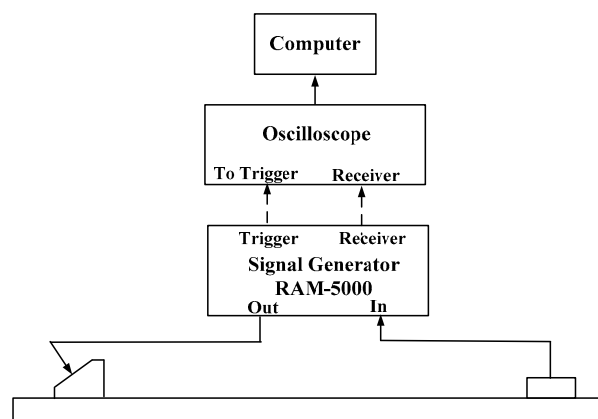
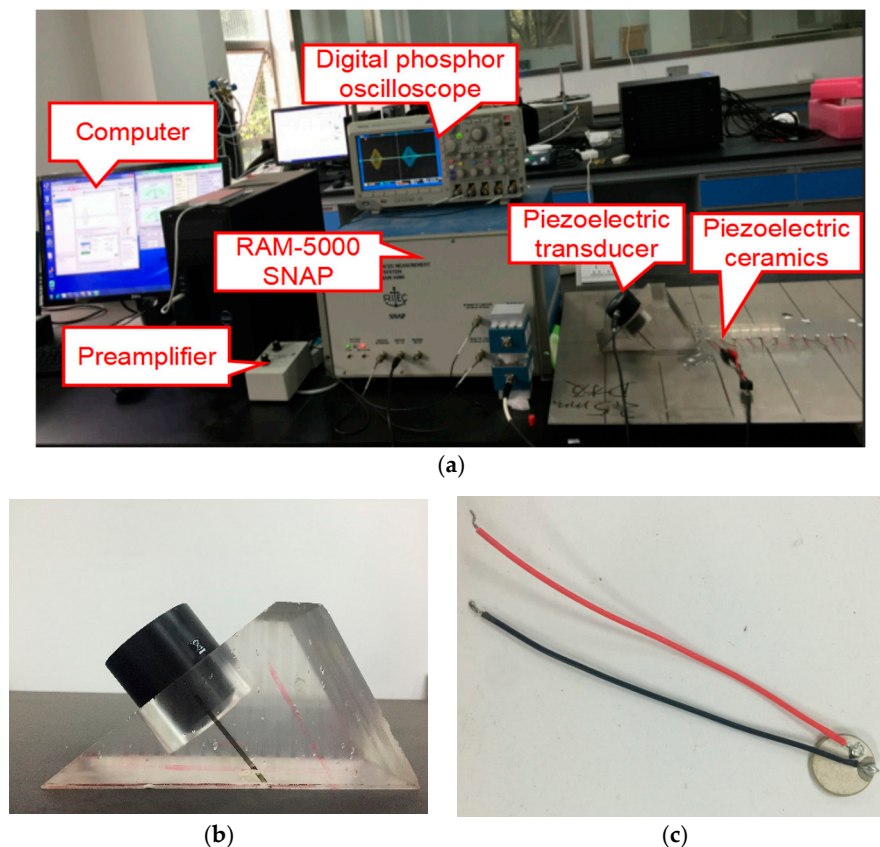


Figure 3. The schematic of the experimental setup.

In experimental measurements, two kinds of aluminum sheets with dimensions of 1.5 mm × 625 mm × 1250 mm and 2 mm × 625 mm × 1250 mm are respectively used for experimental measurements, as shown in Figure 4a. The reference trigger of the DPO 3014 digital phosphor oscilloscope (manufactured by Tektronix Inc., Beaverton, OR, USA) is triggered from the internal trigger signal of RAM-5000 SNAP (Figure 4a). A 10-cycle tone burst of 200V with “Hanning window” generated by RAM-5000 SNAP is fed into the transmitting transducer (Figure 4b), which is attached to the acrylic wedge with the angle 30° to generate  $S_0$  mode waves in aluminum sheets. The wedge is coupled to the transducer and the sheet with Glycerol. The commercial piezoelectric transducer (Model: V1012, Olympus Inc., Tokyo, Japan) with the central frequency of 250 kHz is used as the transmitter. The wave signals propagating in the sheet are received at different positions (see Figure 2) by the piezoelectric ceramics (the type: PSN-33, manufactured by Haiying Inc., Wuxi, China), as shown in Figure 4c, which are adhesively bonded to the sheet. Then the received signals are sent back to the oscilloscope through RAM-5000 SNAP. Finally, the digitized time-domain signals are saved and processed by the computer. Meanwhile, the experimental received data is filtered by both a low-pass filter (20 MHz) and a high-pass filter (50 kHz) by the RAM-5000 SNAP, and average filter (32 times) by the oscilloscope. The received signals are both amplified by a preamplifier (Model: RS-5-G2, RITEC Inc., Warwick, RI, USA) with a −20 dB gain and by a receiver amplifier with a 50 dB gain for 200 kHz and 300 kHz in a 2.0-mm sheet, or by a receiver amplifier with a 40 dB gain for 240 kHz and 300 kHz in a 2.5-mm sheet.



**Figure 4.** (a) The RAM-5000 SNAP nonlinear ultrasonic system; (b) Transmitting transducer; (c) Piezoelectric ceramics (the type: PSN-33).

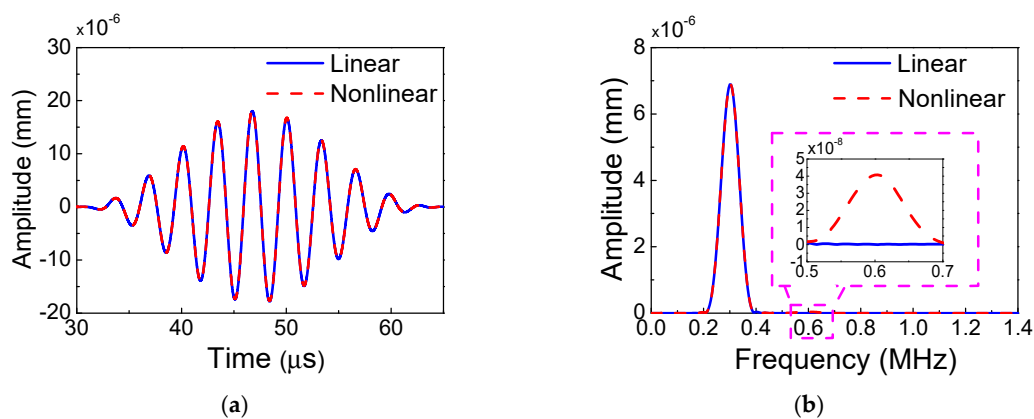
## 5. Result Discussion

Owing to the existing quadratic material nonlinearity, second harmonics can be generated with the propagation of the fundamental  $S_0$  mode waves. In this section, by analyzing the data from numerical simulations and experiments, the effects of different frequency-thicknesses and different frequencies with the same frequency-thickness on dispersion distance are investigated here. Note that the signals of Lamb waves in the  $y$ -direction (the direction perpendicular to the surface of the sheet) are used both for numerical simulations and experiments [41].

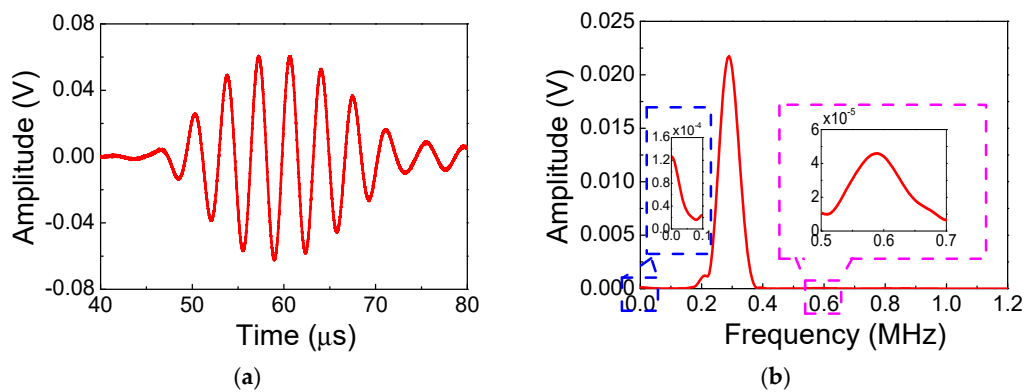
### 5.1. Fundamental Waves and Second Harmonics

Figure 5 shows the signals collected at the location of 120 mm from numerical simulations with frequency-thickness 600 kHz·mm ( $f = 300$  kHz,  $h = 2$  mm), wherein the solid line represents the wave signals for the linear case, and the dashed line represents the wave signals for the nonlinear case. Additionally, the experimental signals collected at the location of 125 mm with the same frequency-thickness are shown in Figure 6. It is found that the time-domain signals of the linear case nearly coincide with that of the nonlinear case as shown in Figure 5a. However, based on the frequency-domain signals with Fast Fourier Transform (FFT), as shown in Figure 5b, we can clearly observe that the wave signals of the nonlinear case marked by the dashed line contain both the fundamental frequency of 300 kHz and the second harmonic 600 kHz. Meanwhile, the signals of the linear case marked by the solid line only contain the fundamental frequency of 300 kHz, indicating that the second harmonic cannot be generated for the linear case. Additionally, the experimental result as shown in Figure 6 demonstrates the same phenomenon. The experimental frequency-domain signals contain not only the second harmonic but also the zero-mode frequency, as shown in Figure 6b. It is found that the amplitude of the second harmonic is rather small. However, this small second

harmonic signal should not be noise since the equipment of RAM-5000 SNAP has a great advantage of being able to acquire the weak harmonics with low-noise, and the amplitude of this small second harmonic can be linearly accumulated during the certain distance. Moreover, the coincident results from repeated experiments are obtained in this work. In addition, the experimental amplitude of zero-mode frequency in the present work is smaller than that in the work of Reference [42] because of the different frequencies (300 kHz in the present work and 200 kHz in the work [42]) and different receiver transducers (piezoelectric ceramics PSN-33 in the present work and Olympus transducer with center frequency 500 kHz in the work of Reference [42]). Here, we find from the numerical simulations and experiments that, when using the low-frequency  $S_0$  mode, weak material nonlinearity is essential to the second harmonic generation of Lamb waves.



**Figure 5.** The signals received at the location of 120 mm from the numerical simulations (a) time domain; (b) frequency domain (Frequency-thickness: 600 kHz·mm).



**Figure 6.** The signals received at the location 125 mm from the experiments (a) time domain; (b) frequency domain (Frequency-thickness: 600 kHz·mm).

## 5.2. The Influence of Frequency-Thickness

In order to obtain repeatable experimental results and eliminate the effect due to the inhomogeneous distribution of the acoustic nonlinearity parameter in the sheet interior, multi-point and repeated measurements are performed in experiments. Each experiment shown in the following is repeated over 40 times. Besides, it should be noted that the wave signals in the distance range (0–100 mm) could not be collected due to the limitations of the experimental equipment.

The different curve fitting types, such as 1st, 2nd, 3rd, 4th, and 5th polynomial, are attempted to fit the numerical and experimental data in Figures 7 and 8. We find that both the 1st and 2nd polynomials are inaccurate, however, the 4th and 5th polynomials show the same accuracy as the 3rd polynomial, which is expressed by a more complex style. Thus, the 3rd polynomial is the best choice of the curve fitting and is employed in Figures 7 and 8 for this work.

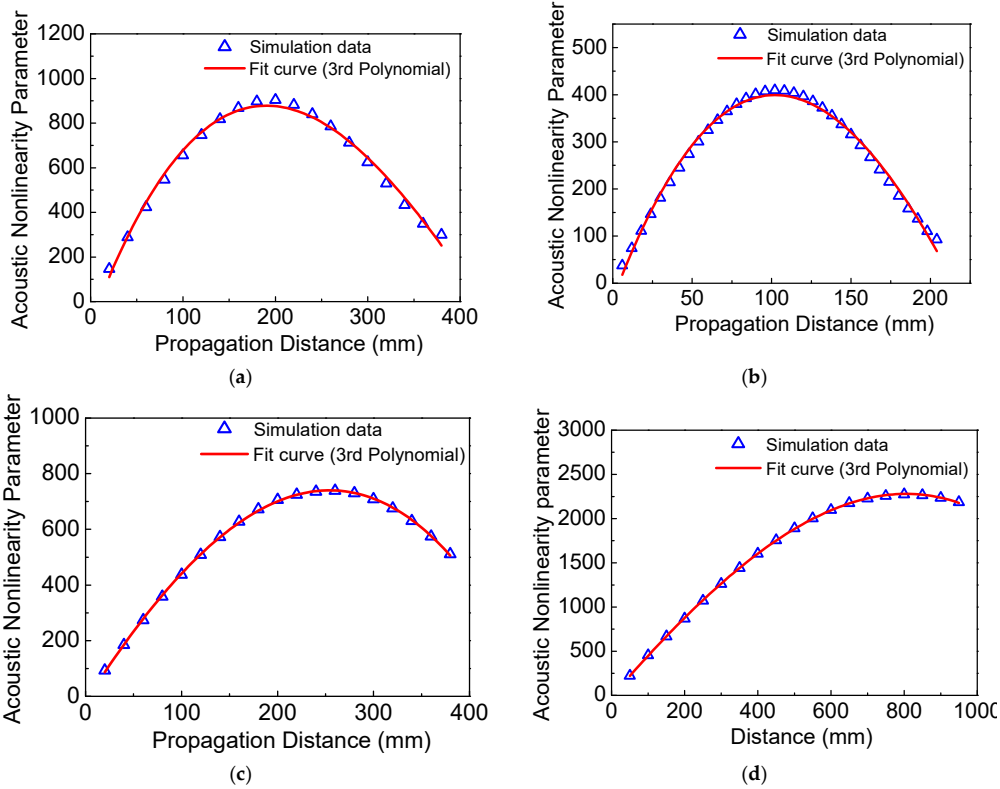


**Figure 7.** The acoustic nonlinearity parameter versus propagation distance from the numerical simulations. (a)  $f = 300$  kHz,  $h = 2.0$  mm; (b)  $f = 300$  kHz,  $h = 2.5$  mm; (c)  $f = 240$  kHz,  $h = 2.5$  mm; (d)  $f = 200$  kHz,  $h = 2.0$  mm.

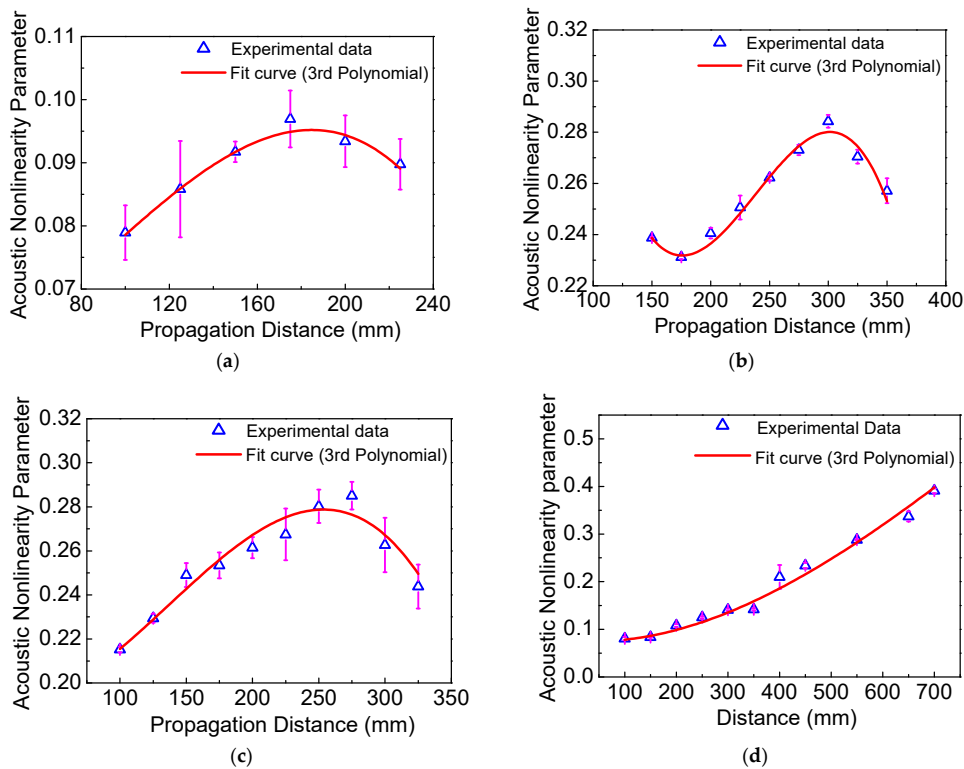


**Figure 8.** The acoustic nonlinearity parameter versus the propagation distance with standard deviations from the experiments (a)  $f = 300$  kHz,  $h = 2.0$  mm; (b)  $f = 300$  kHz,  $h = 2.5$  mm; (c)  $f = 240$  kHz,  $h = 2.5$  mm; (d)  $f = 200$  kHz,  $h = 2.0$  mm.

Figures 7 and 8 show the acoustic nonlinearity parameter versus the propagation distance from the numerical simulations and experiments, respectively. Note that the average values with the associated standard deviations from experiments are shown in Figure 8. It was found that the numerical and experimental results clearly show the sinusoidal behavior as in Figures 7 and 8. Additionally, the dispersion distances obtained from the numerical simulations and experiments for different cases are listed in Table 2, which shows that the experimental results are consistent with those of the numerical simulations.

**Table 2.** The dispersion distances from numerical simulations and experiments.

Case	$L/\text{mm}$ (Numerical Simulations)	$L/\text{mm}$ (Experiments)	Error
$f = 300 \text{ kHz}, h = 2.0 \text{ mm}$	180	175	2.8%
$f = 300 \text{ kHz}, h = 2.5 \text{ mm}$	100	125	25%
$f = 240 \text{ kHz}, h = 2.5 \text{ mm}$	240	250	4.2%
$f = 200 \text{ kHz}, h = 2.0 \text{ mm}$	800	700	12.5%

Meanwhile, we also find that the dispersion distance increases with the decrease of the frequency-thickness, as shown in Table 2. To investigate the relationship between dispersion distance and frequency-thickness, more numerical simulations are carried out here. The acoustic nonlinearity parameter versus frequency-thickness and dispersion distance versus frequency-thickness are shown in Figure 9. Both the acoustic nonlinearity parameter and dispersion distance decrease dramatically with the increase of the frequency-thickness, which are shown as the function of exponential decay. It is clearly shown that both the acoustic nonlinearity parameter and dispersion distance are slightly changed at relatively lower levels over 800 kHz·mm. Therefore, the proper frequency-thickness region should be carefully chosen from 0–800 kHz·mm. Note that, the lower frequency-thickness could raise the sensitivity and the linear accumulative distance, which can provide a feasible theoretical and experimental basis for nonlinear Lamb waves of the low-frequency  $S_0$  mode.

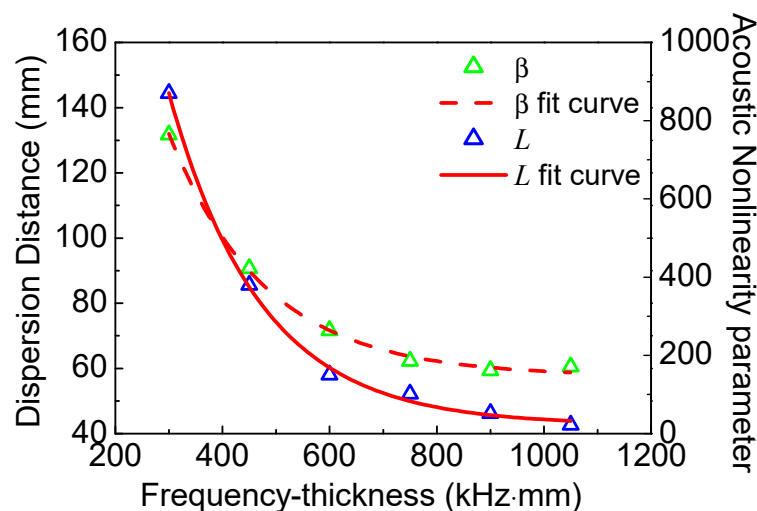


**Figure 9.** The acoustic nonlinearity parameter in the location at 10 mm and the dispersion distance versus frequency-thickness.

Furthermore, an interesting phenomenon can be found from Table 2, revealing the influence of frequency on dispersion distance with the same frequency-thickness. Numerical simulations are also explored to investigate the relationship. With the same frequency-thickness (600 kHz·mm), the acoustic nonlinearity parameter versus frequency and dispersion distance versus frequency are shown in Figure 10. The acoustic nonlinearity parameter shows an exponential increase trend with frequency; however, dispersion distance shows an exponential decay trend with frequency. We can also find that

the acoustic nonlinearity parameter is more sensitive to the frequencies over 200 kHz, but dispersion distance is more sensitive to the frequencies below 400 kHz. Therefore, the appropriate frequency from the range 200–400 kHz could be a compromise considering the influences of sensitivity and linear accumulative distance.

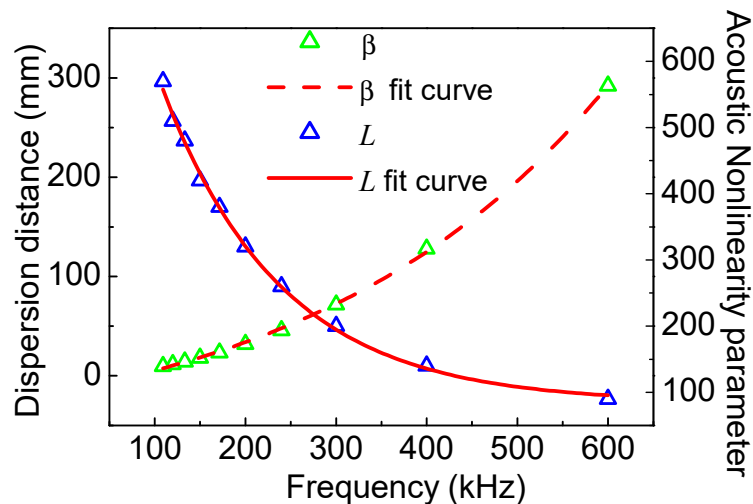


**Figure 10.** The acoustic nonlinearity parameter in the location ay 10 mm and the dispersion distance versus frequency at the same frequency-thickness 600 kHz·mm.

It should be noted that the representative case ( $f = 200$  kHz,  $h = 2.0$  mm) has two great advantages: a lower frequency-thickness (400 kHz·mm) and a lower frequency (200 kHz), which can lead to a higher sensitivity and longer linear accumulative distance. The numerical and experimental results both verify the above-mentioned viewpoints.

## 6. Conclusions

The numerical modeling and experimental investigation in plates with quadratic material nonlinearity are performed to demonstrate the nonlinear phenomena of the low-frequency  $S_0$  mode Lamb wave. The following conclusions are drawn:

Firstly, when the  $S_0$  mode Lamb waves in the low-frequency domain (0–800 kHz·mm) are chosen as the fundamental waves, obvious second harmonics can be observed from the numerical and experimental results. Therefore, the low-frequency domain (0–800 kHz·mm) is an appropriate choice for engineering applications.

Secondly, it is found that both the acoustic nonlinearity parameter and dispersion distance decrease dramatically as the function of exponential decay with the increase of frequency-thickness. Thus, the lower frequency-thickness from 0–800 kHz·mm should be carefully chosen for considering the sensitivity and the linear accumulative distance.

Finally, in the cases of the same frequency-thickness, the appropriate frequency from the range 200–400 kHz could be a compromise considering the influences of sensibility and linear accumulative distance. Additionally, both the numerical and experimental results manifest that the frequency plays a critical role to affect acoustic nonlinearity parameter and dispersion distance. Thus, according to Figures 9 and 10, the appropriate frequency should be carefully chosen in actual NDT applications. This study provides a theoretical and experimental foundation for nonlinear Lamb-wave methods based on the low-frequency  $S_0$  mode.

**Author Contributions:** X.D. wrote the first draft and performed the simulations/experiments, Y.Z. and N.H. revised the paper, Y.L. analyzed the data, J.Z. and M.D. conceived and designed the simulations/experiments.

**Funding:** This work is supported by the National Science Foundation of China (No. 11632004, No. 11604033 and No. 11602040), and Key Program for International Science and Technology Cooperation Projects of Ministry of Science and Technology of China (No. 2016YFE0125900), Key Project of Natural Science Foundation of CQ CSTC (No. cstc2017jcyjBX0063).

**Conflicts of Interest:** The authors declare no conflict of interest.

## References

1. Szilard, J. *Ultrasonic Testing: Nonconventional Testing Techniques*; John Wiley & Sons Ltd.: New York, NY, USA, 1982.
2. Blitz, J.; Simpson, G. *Ultrasonic Methods of Non-Destructive Testing*; Springer Nature: Berlin, Germany, 1995.
3. Drinkwater, B.W.; Wilcox, P.D. Ultrasonic arrays for non-destructive evaluation: A review. *NDT E Int.* **2006**, *39*, 525–541. [[CrossRef](#)]
4. Cantrell, J.H.; Yost, W.T. Nonlinear ultrasonic characterization of fatigue microstructures. *Int. J. Fatigue* **2001**, *23*, 487–490. [[CrossRef](#)]
5. Ogi, H.; Hirao, M.; Aoki, S. Noncontact monitoring of surface-wave nonlinearity for predicting the remaining life of fatigued steels. *J. Appl. Phys.* **2001**, *90*, 438–442. [[CrossRef](#)]
6. Nagy, P.B. Fatigue damage assessment by nonlinear ultrasonic materials characterization. *Ultrasonics* **1998**, *36*, 375–381. [[CrossRef](#)]
7. Donskoy, D.; Zagrai, A.; Chudnovsky, A.; Golovin, E.; Agarwala, V.S. Assessment of incipient material damage and remaining life prediction with nonlinear acoustics. *J. Acoust. Soc. Am.* **2006**, *119*, 3293. [[CrossRef](#)]
8. Li, W.; Cho, Y.; Achenbach, J.D. Detection of thermal fatigue in composites by second harmonic Lamb waves. *Smart Mater. Struct.* **2012**, *21*, 85–93. [[CrossRef](#)]
9. Biwa, S.; Nakajima, S.; Ohno, N. On the acoustic nonlinearity of solid-solid contact with pressure-dependent interface stiffness. *J. Appl. Mech.* **2004**, *71*, 508–515. [[CrossRef](#)]
10. Cantrell, J.H. Fundamentals and applications of nonlinear ultrasonic nondestructive evaluation. In *Ultrasonic Nondestructive Evaluation*; CRC Press: Boca Raton, FL, USA, 2004; pp. 363–434.
11. Chillara, V.K.; Lissenden, C.J. Nonlinear guided waves in plates: A numerical perspective. *Ultrasonics* **2014**, *54*, 1553–1558. [[CrossRef](#)] [[PubMed](#)]
12. Shen, Y.; Giurgiutiu, V. WaveFormRevealer: An analytical framework and predictive tool for the simulation of multi-modal guided wave propagation and interaction with damage. *Struct. Health Monit.* **2014**, *13*, 491–511. [[CrossRef](#)]
13. Shen, Y.; Giurgiutiu, V. Predictive modeling of nonlinear wave propagation for structural health monitoring with piezoelectric wafer active sensors. *J. Intell. Mater. Syst. Struct.* **2014**, *25*, 506–520. [[CrossRef](#)]
14. Solodov, I.Y.; Krohn, N.; Busse, G. CAN: An example of nonclassical acoustic nonlinearity in solids. *Ultrasonics* **2002**, *40*, 621–625. [[CrossRef](#)]
15. Lu, Y.; Ye, L.; Su, Z.; Yang, C. Quantitative assessment of through-thickness crack size based on Lamb wave scattering in aluminium plates. *NDT E Int.* **2008**, *41*, 59–68. [[CrossRef](#)]
16. Shen, Y.; Cesnik, C.E.S. Modeling of nonlinear interactions between guided waves and fatigue cracks using local interaction simulation approach. *Ultrasonics* **2016**, *74*, 106–123. [[CrossRef](#)] [[PubMed](#)]
17. Deng, M.-X.; Yang, J. Characterization of elastic anisotropy of a solid plate using nonlinear Lamb wave approach. *J. Sound Vib.* **2007**, *308*, 201–211. [[CrossRef](#)]
18. Deng, M.; Xiang, Y.; Liu, L. Time-domain analysis and experimental examination of cumulative second-harmonic generation by primary Lamb wave propagation. *J. Appl. Phys.* **2011**, *109*, 113525. [[CrossRef](#)]
19. Matsuda, N.; Biwa, S. Phase and group velocity matching for cumulative harmonic generation in Lamb waves. *J. Appl. Phys.* **2011**, *109*, 094903. [[CrossRef](#)]
20. Li, M.; Deng, M.; Gao, G.; Xiang, Y. Mode pair selection of circumferential guided waves for cumulative second-harmonic generation in a circular tube. *Ultrasonics* **2018**, *82*, 171–177. [[CrossRef](#)] [[PubMed](#)]
21. Matlack, K.H.; Kim, J.-Y.; Jacobs, L.J.; Qu, J. Experimental characterization of efficient second harmonic generation of Lamb wave modes in a nonlinear elastic isotropic plate. *J. Appl. Phys.* **2011**, *109*, 014905. [[CrossRef](#)]

22. Li, M.; Deng, M.; Gao, G.; Xiang, Y. Modeling of second-harmonic generation of circumferential guided wave propagation in a composite circular tube. *J. Sound Vib.* **2018**, *421*, 234–245. [[CrossRef](#)]
23. Bermes, C.; Kim, J.-Y.; Qu, J.; Jacobs, L.J. Experimental characterization of material nonlinearity using Lamb waves. *Appl. Phys. Lett.* **2007**, *90*, 021901. [[CrossRef](#)]
24. Bermes, C.; Kim, J.-Y.; Qu, J.; Jacobs, L.J. Nonlinear Lamb waves for the detection of material nonlinearity. *Mech. Syst. Signal Process.* **2008**, *22*, 638–646. [[CrossRef](#)]
25. Müller, M.F.; Kim, J.-Y.; Qu, J.; Jacobs, L.J. Characteristics of second harmonic generation of Lamb waves in nonlinear elastic plates. *J. Acoust. Soc. Am.* **2010**, *127*, 2141–2152. [[CrossRef](#)] [[PubMed](#)]
26. Matlack, K.H.; Kim, J.-Y.; Jacobs, L.J.; Qu, J. Review of second harmonic generation measurement techniques for material state determination in metals. *J. Nondestruct. Eval.* **2015**, *34*, 273. [[CrossRef](#)]
27. Wan, X.; Tse, P.W.; Xu, G.H.; Tao, T.F.; Zhang, Q. Analytical and numerical studies of approximate phase velocity matching based nonlinear S0 mode Lamb waves for the detection of evenly distributed microstructural changes. *Smart Mater. Struct.* **2016**, *25*, 045023. [[CrossRef](#)]
28. Zuo, P.; Zhou, Y.; Fan, Z. Numerical and experimental investigation of nonlinear ultrasonic Lamb waves at low frequency. *Appl. Phys. Lett.* **2016**, *109*, 021902. [[CrossRef](#)]
29. Castaings, M.; Le Clezio, E.; Hosten, B. Modal decomposition method for modeling the interaction of Lamb waves with cracks. *J. Acoust. Soc. Am.* **2002**, *112*, 2567–2582. [[CrossRef](#)] [[PubMed](#)]
30. Liu, X.F.; Bo, L.; Liu, Y.L.; Zhao, Y.X.; Zhang, J.; Hu, N.; Fu, S.Y.; Deng, M.X. Detection of micro-cracks using nonlinear lamb waves based on the Duffing-Holmes system. *J. Sound Vib.* **2017**, *405*, 175–186. [[CrossRef](#)]
31. Jiao, J.; Meng, X.; He, C.; Wu, B. Nonlinear Lamb wave-mixing technique for micro-crack detection in plates. *NDT E Int.* **2016**, *85*, 63–71.
32. Ishii, Y.; Biwa, S.; Adachi, T. Non-collinear interaction of guided elastic waves in an isotropic plate. *J. Sound Vib.* **2018**, *419*, 390–404. [[CrossRef](#)]
33. Li, F.; Zhao, Y.; Cao, P.; Hu, N. Mixing of ultrasonic Lamb waves in thin plates with quadratic nonlinearity. *Ultrasonics* **2018**, *87*, 33–43. [[CrossRef](#)] [[PubMed](#)]
34. Zhu, W.; Xiang, Y.; Liu, C.-J.; Deng, M.; Ma, C.; Xuan, F.-Z. Fatigue damage evaluation using nonlinear Lamb Waves with Quasi phase-velocity matching at low frequency. *Materials* **2018**, *11*, 1920. [[CrossRef](#)] [[PubMed](#)]
35. Hasanian, M.; Lissenden, C.J. Second order harmonic guided wave mutual interactions in plate: Vector analysis, numerical simulation, and experimental results. *J. Appl. Phys.* **2017**, *122*, 084901. [[CrossRef](#)]
36. Liu, X.; Bo, L.; Liu, Y.; Zhao, Y.; Zhang, J.; Deng, M.; Hu, N. Location identification of closed crack based on Duffing oscillator transient transition. *Mech. Syst. Signal Process.* **2018**, *100*, 384–397. [[CrossRef](#)]
37. Radecki, R.; Su, Z.; Cheng, L.; Packo, P.; Staszewski, W.J. Modelling nonlinearity of guided ultrasonic waves in fatigued materials using a nonlinear local interaction simulation approach and a spring model. *Ultrasonics* **2018**, *84*, 272–289. [[CrossRef](#)]
38. Liu, Y.; Kim, J.-Y.; Jacobs, L.J.; Qu, J.; Li, Z. Experimental investigation of symmetry properties of second harmonic Lamb waves. *J. Appl. Phys.* **2012**, *111*, 053511. [[CrossRef](#)]
39. Zhao, Y.; Chen, Z.; Cao, P.; Qiu, Y. Experiment and FEM study of one-way mixing of elastic waves with quadratic nonlinearity. *NDT E Int.* **2015**, *72*, 33–40. [[CrossRef](#)]
40. Lima, W.J.N.D.; Hamilton, M.F. Finite-amplitude waves in isotropic elastic plates. *J. Sound Vib.* **2003**, *265*, 819–839. [[CrossRef](#)]
41. Zhao, Y.X.; Li, F.L.; Cao, P.; Liu, Y.L.; Zhang, J.Y.; Fu, S.Y.; Zhang, J.; Hu, N. Generation mechanism of nonlinear ultrasonic Lamb waves in thin plates with randomly distributed micro-cracks. *Ultrasonics* **2017**, *79*, 60–67. [[CrossRef](#)] [[PubMed](#)]
42. Sun, X.; Ding, X.; Li, F.; Zhou, S.; Liu, Y.; Hu, N.; Su, Z.; Zhao, Y.; Zhang, J.; Deng, M. Interaction of Lamb wave modes with weak material nonlinearity: Generation of symmetric zero-frequency mode. *Sensors* **2018**, *18*, 2451. [[CrossRef](#)] [[PubMed](#)]

